`

Nonlinear finite element analysis for Concrete Deep Beam Reinforced with GFRP Bars

ABSTRACT

This work investigates the behavior of concrete deep beams reinforced with GFRP bars by conducting an experimental test on a half-scale GFRP deep beam and evaluating the findings by ANSYS software. Also, ANSYS was used to perform nonlinear finite element analysis NLFEA on five specimens with different reinforcement ratios of GFRP bars (0.15%, 0.41%, 0.53%, 0.67%, and 0.79%) to examine the influence of the GFRP reinforcement ratio on the behavior of deep beams. The outcomes of the experiment were sufficiently reflected in the analysis. The program's viability was confirmed by comparing it to accessible experimental data, and the agreement was found to be acceptable. Throughout the loading stages, the NLFEA produced a reasonable estimate of the center deflection for the test specimen. It was established that raising the specimen's reinforcement ratio led to an increase in beam capacity by (10 %, 18%, 31% and 47%) for reinforcement ratios (0.41%, 0.53%, 0.67% and 0.79%) and also the ultimate stiffness increased by (6%, 7%, 29%, and 44%) compared to specimen B1. Also found that the energy absorption enhanced by (23 %, 38 %, 106 %, and 152 %), on the opposite, this increase causes the specimen's deflection to decrease by (11 %, 17%, 52%, and 66%) by comparing to specimen B1. From the outputs results, it was found that the code provision was more conservative than the analytical model. For future work, Significant and cost-effective improvements to the manufacture of GFRP bars from locally sourced raw materials. Also, Extensive experimental work to investigate the long-term behavior of GFRP-reinforced concrete beams in harsh situations. The performance of GFRP reinforced specimens subjected to shear, fatigue, and cyclic stresses in service must be evaluated.

KEYWORDS: DEEP BEAMS; GFRB; FINITE ELEMENT.

1. INTRODUCTION

In the civil and structural engineering sectors, composite materials, such as Fiber Reinforced Polymer (FRP) bars, have been gaining traction as alternatives to traditional steel reinforcements (FRP) materials are non-corrosive, making them an excellent substitute for steel reinforcement in harsh conditions. They are also lightweight and have a high longitudinal tensile strength. [1]. The long-term endurance of the reinforced concrete

`

structures has become a key problem in the building industry. One of the leading reasons of structure made of reinforced concrete service life reduction is the rapid Steel reinforcing bars corrode. Tanks, dams, and bridges, for example, were subjected to dampness, chlorides, and de-icing salts, which corroded steel reinforcement. Steel reinforcing bars should be changed or coated with non-corrosive materials to solve this problem and meet the requirements for ultimate limit state and durability for these buildings.

Fiber reinforced polymer (FRP) bars recently they've been used as an alternate material. To the steel reinforcement bars that have corroded. Carbon (CFRP), glass (GFRP), and aramid fibers are the most popular forms of fibers (AFRP). FRP bars have a good corrosion resistance and a high specific strength. Corrosion of steel reinforcement in concrete constructions causes concrete to crack and spall, requiring expensive maintenance and repair. As a result, by replacing the steel reinforcement with non-corrosive (FRP) reinforcement, the possibility of corrosion and subsequent deterioration is eliminated [2].

Many steel-reinforced concrete structures, such as bridges, parking garages, and offshore vessels, are subjected to harsh environments that, over time, can cause substantial damage and necessitate costly rehabilitation due to steel reinforcement corrosion. Extensive study has been conducted on the behavior of slender (shallow) concrete elements reinforced with (FRP) reinforcement. [3]. A deep beam is a member with a small shear span-to-depth (a/d) ratio [4]. In another words, a beam with a (a/d) ratio of less than 4 can be considered a deep beam [5].

Matthias et al. [3] presented a twelve-large-scale beam experimental examination. The specimens' height, shear span-to-depth (a/d) ratio, reinforcing ratio (ρ), and concrete compressive strength (fc) were the main factors. To investigate the concrete contribution to shear capacity, no distributed or transverse web reinforcing was incorporated in the tested specimens. The (GFRP) bars provided longitudinal reinforcement. When the reinforcement ratio was raised, the normalized shear capacity improved by 3%. Reduced normalized shear stress at the ultimate load is a result of increased member height. By increasing concrete strength, the normalized shear capacity decreases.

Ahmed et al. [6] investigated the behavior of the shear of four full-scale carbon fiber reinforced plastic deep beams. (CFRP) and glass fiber reinforced plastic (GFRP) bars. The key test factors were the ratio of the tension reinforcement bars and the type of reinforcement. The ultimate capacity and deflection were significantly affected by the reinforcement ratio

and concrete compressive strength, whereas the reinforcement type had no discernible effect on the behavior of the tested beams. All of the test beams failed due to brittle failure.

2. Experimental program

2.1. Test specimen

One half-scale GFRP reinforced concrete deep beam with an acceptable degree of longitudinal and shear reinforcement was built as a simply supported span. As tension reinforcement, 2 ϕ16 GFRP bars were added to the specimen. To hold the stirrups, two 12 mm high tension steel bars were used as top reinforcement. 10 mm diameter vertical stirrups @ 100 mm c/c spacing, and three 10 mm diameter horizontal stirrups were used as shear reinforcement. The 16 mm diameter GFRP bars had an ultimate strength of around 850 MPa. In addition, the concrete's cubic compressive strength ($f$cu) was 25 MPa. This study looked into the effects of using GFRP bars as reinforcement bars on the behavior of reinforced concrete deep beams. The mean stress-strain curve for GFRP bars is shown in Figure. 1. The arrangement of the tested beam is shown in Figure. 2

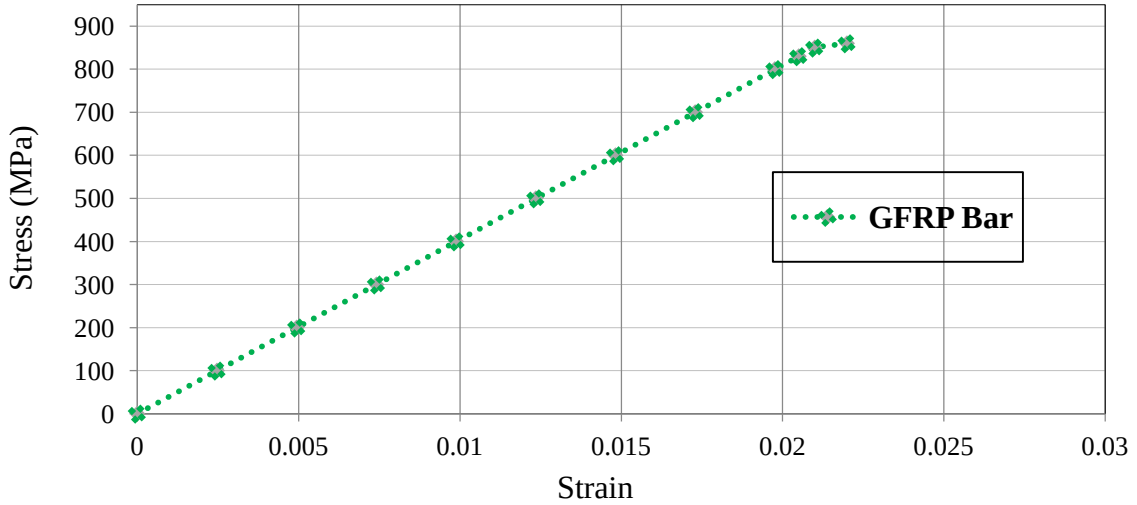

Figure 1 The mean stress-strain curve for GFRP bars.

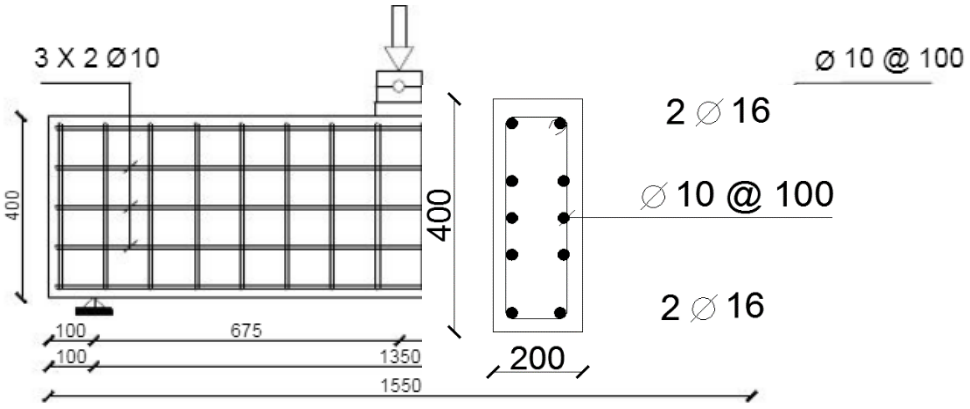

`

Figure 2 Tested Beam Geometry and Details.

2.2. Test setup

The specimen were placed through the test under load control. Electrical resistance strain gauges were employed to assess the reinforcement's strain in major points [7]. Where it is placed at the longitudinal and shear reinforcement bars to determine the strain of the bars, as illustrated in Figure. 3. Deflections of the experimentally tested specimen are measured and monitored using linear variable differential transformers (LVDT) connected to the specimen at the mid- span [8] as shown in Figure. 4. The cracks were marked during the loading stages till the specimen failed. The deep beam was tested in a machine of 650 kN capacity. The load was concentrated on one plate. The loads was symmetrical to the centerline of the deep beam.

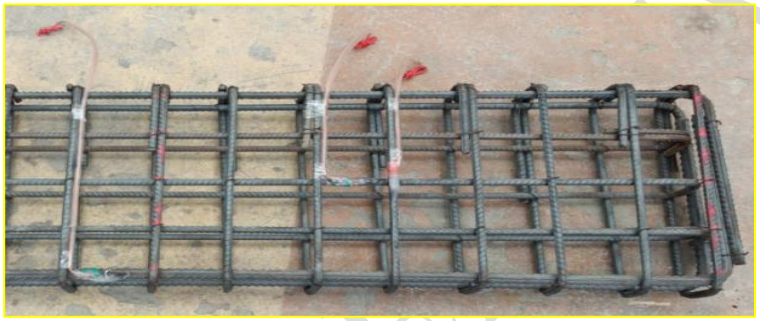

Figure 3. Installation of strain gauges.

Figure 4. LVDT installation.

`

3. Experimental results and discussion

3.1. Crack and ultimate load and Crack pattern

The deep beam was visually observed until reach the first crack appeared, with the corresponding first crack load being recorded. The initial crack in this beam occurred in the compression zone, and it was a shear inclined crack. The flexure cracks in the tension area will have to appear quickly. As the load increases, the deflection of the beam increases rapidly. As the applied load increases, the primary shear crack linking the loading plate to the right side support will develop. As demonstrated by the cracking pattern, the concrete just below the loading plate is crushed, resulting in a significant reduction in load-carrying capacity. At final level, the brittle failure happens suddenly and the mode of failure of this specimen was shear compression failure. The crack pattern for experimental tested specimen B at failure is shown in Figure. 5.

Figure 5. Cracks pattern for experimental tested specimen B at failure.

`

4. Non-Linear Finite Elements Analysis (NLFE)

NLFEA was utilized to model the tested concrete deep beams. [9]. ANSYS (ANSYS release 12.1) [10], a commercially accessible finite element (FE) analysis software program, was used.

4.1. Finite Element Formulation

The 3-D model for a typical deep beam is presented in Figure.6. Solid 65 for concrete is the structural element type utilized for geometric idealization of the diverse materials because of its ability to plastic deformation, cracking, and crushing in three directions. For idealized reinforcing bars and stirrups, 3-D spar elements (Link 8) were employed. It has two node and three DOF. It also has the ability to deform plastically [9]. The Hognestad-Popvics stress–strain curve [11] was utilized for concrete in compression. A linear-tension curve was utilized for concrete in tension [12]. The bilinear stress–strain curve was employed for steel reinforcement in tension and compression [13], while the (GFRP) bars had a linear elastic behavior. The concrete and bars were thought to have a perfect connection.

Five deep beam specimens (B1, B2, B3, B4 and B5) of rectangular shape with dimensions of 200X400X1550 mm was presented. These specimens were reinforced with different reinforcement ratios of GFRP bars (0.15%, 0.41%, 0.53%, 0.67% and 0.79%). It should be noted that the specimen B3 with 2ϕ16 GFRP bars corresponds to the specimen B that was experimentally tested. This specimen considered as a control specimen to verify the experimental results.

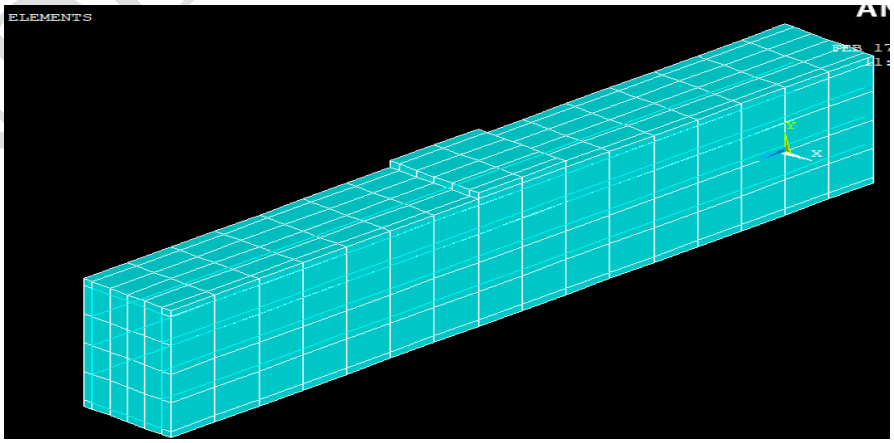

(a) Concrete Element; Solid65

`

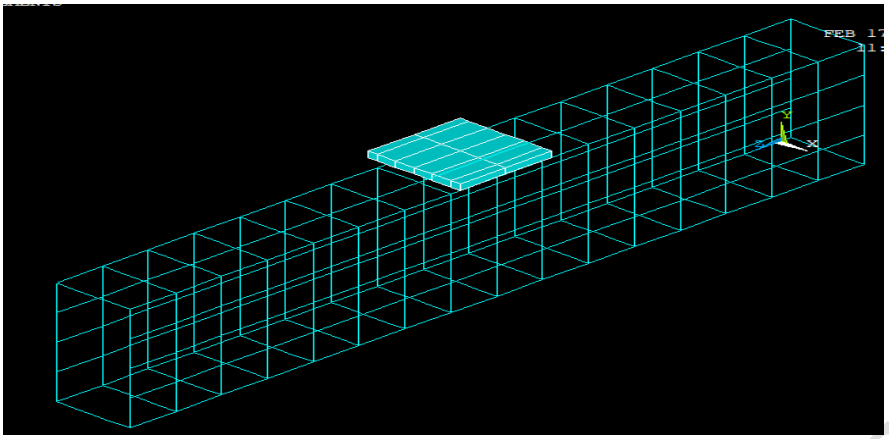

(b) Reinforcing Bar Element; Link8

Figure 6. Models for the Tested Deep Beams based on Finite Element Simulation.

4.2. Analytical procedures

An incremental load approach was used to accommodate for non-linear analysis in the numerical solution scheme. The iterative solution used for each load increment was a blend of the traditional Newton-Raphson method's high convergence rate and the low cost of the modified Newton-Raphson approach, in which the stiffness was reformulated every loading step. Only transitory degrees of freedom were considered in the convergence criterion, which was based on iterative nodal displacement. The criterion is:

$$\psi / R \leq \phi$$

where ψ is the iterative displacement norm and R is the total displacement norm. The convergence tolerance, which ϕ was discovered to be between 0.01 and 0.05, produced satisfactory results. The analytical ultimate load of the test specimen has been defined as the load level at which the convergence criteria was not met, suggesting numerical instability [14].

5. Results of non-linear finite element analysis

5.1. Crack patterns

Figure. 7 shows the NLFEA outputs, which depict the crack pattern of the five GFRP tested specimens analytically with deferent ratios of GFRP bars. By noting the shape of the crack patterns, It can be demonstrated that increasing the ratio of reinforcement bars increases the ultimate load that the specimen can carry, and hence increasing crack propagation along the

`

beams. It's also worth mentioning that analytically tested specimen B3 corresponds to specimen B which tested experimentally. The cracks began to emerge in the compression zone, as shear cracks, and with the increase in loads, the cracks began to propagate and extend in the area linking the loading plate and support at wider perimeters, It largely agrees with the results of the experiments. Crack development and propagation patterns were comparable in all beams.

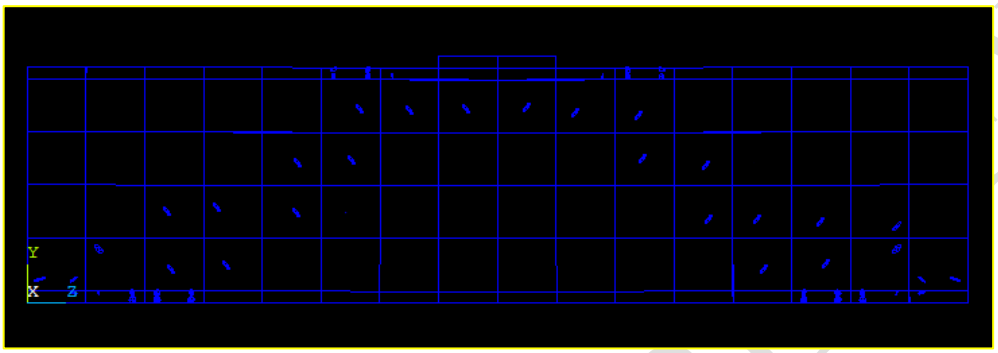

(a) B1.

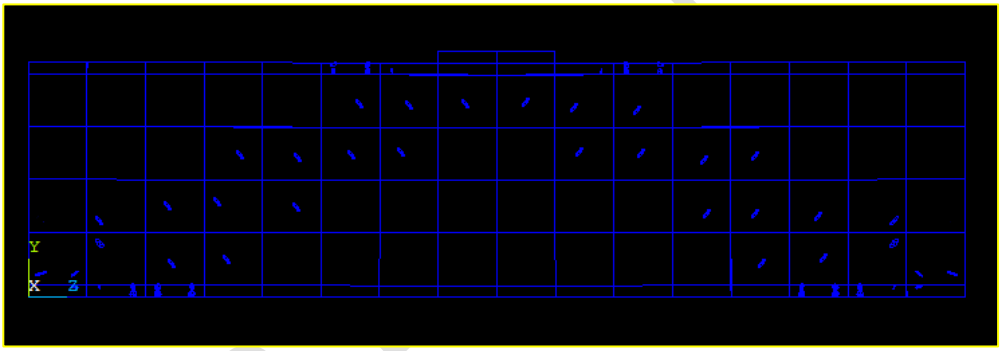

(b) B2.

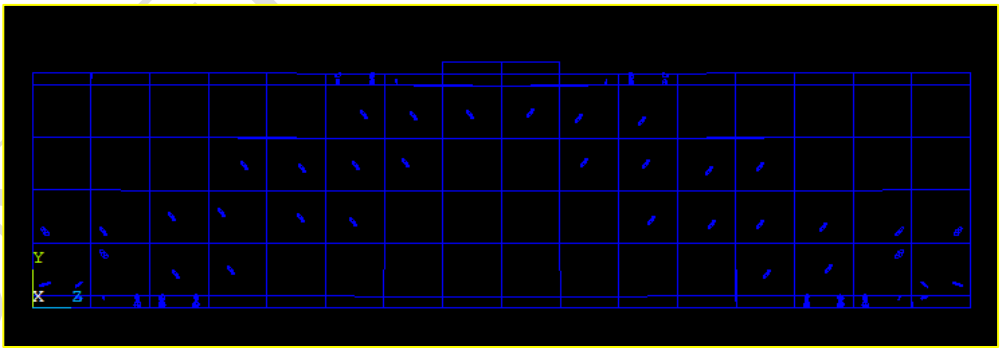

(c) B3.

`

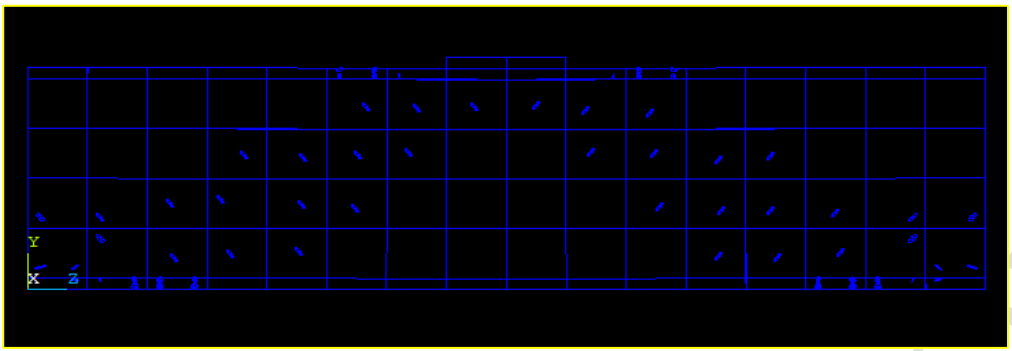

(d) B4.

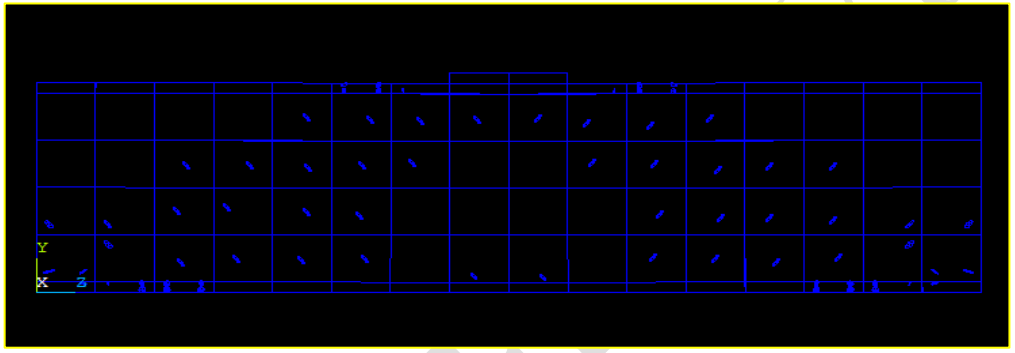

(d) B5.

Figure 7. Predicted Crack Pattern for Beams B1, B2, B3, B4 and B5.

5.2.Load-deflection behavior

The load–deflection curve is an important factor of beam behavior verification. It includes beneficial parameter which is the ratio of (GFRP) bars. According to Figure.8, for the experimentally tested specimen B, the NLFEA provided a fair estimate of the central deflection throughout the loading stages. It was discovered that the curve of specimen B is split into two parts, the first of which exhibits rather linear elastic behavior up to the cracking load when the concrete cracked at the tension face. Second is the nonlinear phase, which is the load grows with the steady increase in deflection until the ultimate load reached. Then the curve start decreasing, where the specimen become unable to sustain more loads, therefore the load gradually decreases as the deflection increases until it reaches the failure point. It's worth noting that the drop that happened in the curve was caused by an oil release in the hydraulic jack, which was repaired before the tested specimen was returned to its proper loading position and able to receive additional loads and drop points was removed from the curve.

Five specimens of deep beams that reinforced with varied ratios of reinforcing bars were developed when it was discovered that the model achieved and confirmed the experimental test as shown in Figure.9. Which represent that the all of analytical GFRP reinforced beams had bilinear loads-mid span deflection curves. The behavior of un-cracked beams is shown by the first half of the curve up to the point of cracking. The behavior of cracked beams with lower stiffness is depicted in the second part. Furthermore, it was clear that the reinforcement ratio had an impact on the load deflection response of analytical deep beam specimens. Whereas at the same level of loading, deflection decreased as the reinforcement ratio increased. Compared to specimen B1, when the ultimate load in the specimens B2, B3, B4 and B5 was increased by 10 %, 18%, 31% and 47% respectively. This resulted in a reduction in deflection by 11 %, 17%, 52% and 66% respectively.

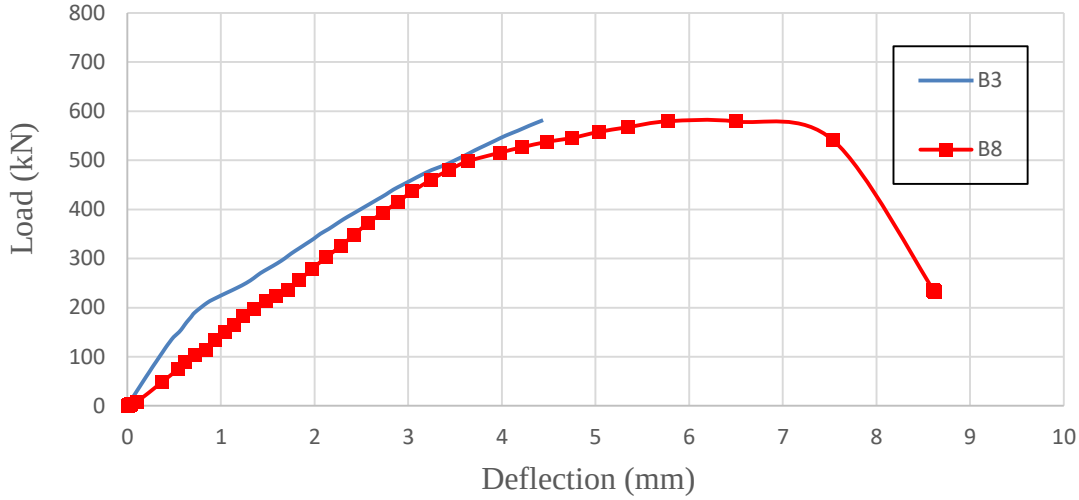

Figure 8. Load deflection relationship for specimens B3 and B at failure.

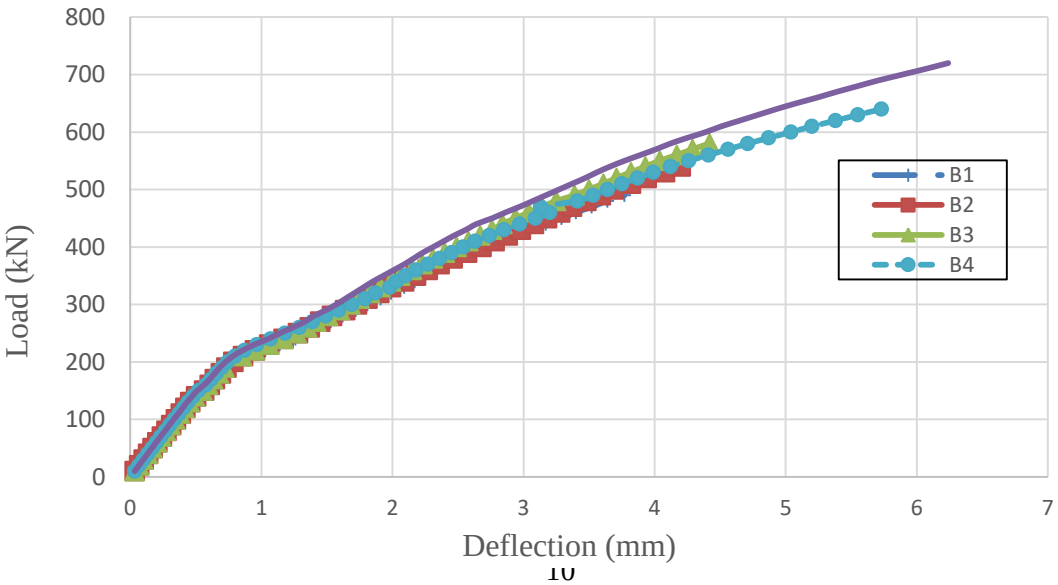

`

Figure 9. Load deflection relationship for analytical deep beam specimens at failure.

5.3. Ultimate failure load

Table. 1 shows the analytical ultimate failure loads (*Fa*) and the ACI318-08 predicted values (*Fp*) without any safety factor. The ratio of predicted strength to analytical strength varied between 0.58 and 0.73. The ACI provisions' had a conservative prediction more than analytical model.

Table.1 Comparison of the Analytical ultimate loads and predicted values.

Specimen	Reinforcement ratio (%)	Beam dimension, mm	Analytical failure load, *Fa*, kN	Predicted failure load, *Fp* (ACI), kN	*Fp/Fa*
B1	0.15	200 x 400	500	290	0.58
B2	0.41	200 x 400	540	329	0.61
B3	0.53	200 x 400	580	383	0.66
B4	0.67	200 x 400	640	454	0.71
B5	0.79	200 x 400	720	526	0.73

`

5.4.Stiffness

According to Marzouk and Hussein (1991) [15], the stiffness of specimens tested can be assessed as follows: The initial stiffness (*Ki*) defined as the slope of the load-deflection curve at the start of the curve, whereas the ultimate stiffness (*Ku*) is the slope of the load-deflection curve at nearly 90% of peak load. Consequently, the ratio of ultimate stiffness to initial stiffness (*Ku/Ki*) is used to describe stiffness degradation. The initial, ultimate, and stiffness degradation ratios for five analytical specimens are shown in Table. 2. The results show that the initial, ultimate, and stiffness degradation increased as the ratio of GFRP bars rose for all specimens. In comparison to B1, the ultimate stiffness of specimens B2, B3, B4, and B5 rose by 6%, 7%, 29%, and 44%, respectively. Accordingly, the stiffness degradation also increased by 11%, 21%, 32% and 53% respectively. Beams reinforced with GFRP bars give high values to stiffness due to the high strength of these bars.

Table. 2 Stiffness results of analytical specimens.

Specimen	Initial stiffness; *Ki* (kN/mm)	Ultimate stiffness; *Ku* (kN/mm)	Stiffness Degradation Ratio;*Ku/Ki*
B1	306.16	58.17	0.19
B2	293.20	61.53	0.21
B3	269.83	62.06	0.23
B4	300.56	75.14	0.25
B5	289.72	84.02	0.29

5.5. Energy absorption

The area beneath the load–deflection curve is referred to as energy absorption. It's a result of the ultimate load and the ultimate deflection that goes along with it [16]. Table.3 shows the energy absorbed for analytical specimens. In general, raising the GFRP bars reinforcing ratio improved energy absorption for analytically tested specimens B2, B3, B4, and B5 had higher energy absorption than B1, by 23 %, 38 %, 106 %, and 152 %, respectively.

`

Table.3 Energy absorption results of analytical specimens.

Specimen	Energy absorption (kN.mm)
B1	1122.2
B2	1374.7
B3	1548.9
B4	2316.9
B5	2829.8

6. Conclusions

Analytical study of five deep beam specimens of GFRP bars ratio varied between 0.15% and 0.79% was investigated. Based on the analytical results and the comparison with the experimental study on one deep beam specimen and ACI code provision values in this study, the main conclusion points can be drawn as follows:

1. Generally, the provision of the GFRP reinforcement bars enhanced the capacity of the deep beams due to the high strength of these bars.
2. Reinforcement ratio exhibited a noticeable effect on the behavior of deep beams.
3. For the analytically tested GFRP beams, the loads' deflection curve was bilinear. The initial half of the curve up to the point of cracking depicts the behavior of uncracked beams. The behavior of broken beams with lower rigidity is depicted in the second part.
4. The load deflection curve for the beam obtained from finite element calculations reflect the experimental data rather well.
5. When comparing the results of the analytic research and the experimental test for two specimens B and B3, there is a good agreement in the outputs.
6. The load-carrying capacity and stiffness of GFRP beams were improved by increasing the reinforcement ratio. On the contrary, the deflection was reduced by (11 %, 17%, 52% and 66%) for specimens B2, B3, B3, B4 and B5 respectively compared to specimen B1.
7. The addition of the GFRP bars improved the energy absorption, according to the

`

results of analytical specimens. This is made possible by the GFRP bars' high strength, which results in a high beam capacity and hence higher energy absorption.

8. The energy absorption enhanced by (23 %, 38 %, 106 %, and 152 %) for specimens B2, B3, B4 and B5 respectively compared to the specimen B1.

9. Reinforcement ratio should be adopted in deep beams formula as significant factor.

10. When compared to analytical values, ACI provisions indicated a fairly conservative final capacity.

7. References

1. ACI Committee 318, "Building Code Requirements for Structural Concrete (ACI 318-05) and Commentary (318R-05)," American Concrete Institute, Farmington Hills, MI, 2005, 430 pp.
2. Moe, J., "Shearing Strength of Reinforced Concrete Slabs and Footings Under Concentrated Loads," Bulletin No. D47, Journal of the Portland cement Association, Research and Development Laboratories, Apr. 1961, 130 pp.
3. Joint ACI-ASCE Committee 326, "Shear and Diagonal Torsion," ACI Structural Journal, V. 85, No. 6, Nov.-Dec. 1988, pp. 675-696.
4. Regan, P. E., and Bræstrup, M. W., "Punching Shear in Reinforced Concrete," Bulletin d'Information No. 168, Comité Euro-International du Béton, Jan. 1985, 232 pp.
5. Regan, P. E., "Symmetric Punching of Reinforced Concrete Slabs," Magazine of Concrete Research, V. 38, No. 136, Sept. 1986, pp. 115-128.
6. Bažant, Z. P., and Cao, Z., "Size Effect in Punching Shear Failure of Slabs," ACI Structural Journal, V. 84, No. 6, Jan.-Feb. 1987, pp. 44-53.
7. Moran, J. D. D. G., & de Dios, J. (2009). Behaviour of concrete deep beams with high strength reinforcement. Library and Archives Canada= Bibliothèque et Archives Canada, Ottawa.
8. Ali, S. S. (2014). Behavior of Concrete Beams Reinforced with GFRP Bars (Doctoral dissertation, Ph. D. Dissertation, Faculty of Engineering, Shoubra, Benha University, Cairo, Egypt).
9. Said, M., Shanour, A. S., Mustafa, T. S., Abdel-Kareem, A. H., & Khalil, M. M. (2021). Experimental flexural performance of concrete beams reinforced with an innovative hybrid bars. Engineering Structures, 226, 111348.

`

10. ANSYS–Release Version 12.1.0. A Finite Element Computer Software and User Manual for Nonlinear Structural Analysis. Canonsburg, PA: ANSYS Inc; 2009.
11. Montoya E, Vecchio F, Sheikh SA. Compression field modelling of confined concrete. J Struct Eng Mech 2001;12(3).
12. Careira DJ, Chu KH. Stress-strain relationship of reinforced concrete in tension. ACI Mater J 1990;83:21–8.
13. Eurocode 3. Design of Steel Structures, ENV EC3 Part 1.2.“, Eurocode; 2005.
14. Abdel-Fttah, A., Said, M., & Salah, A. (2016). Nonlinear finite element analysis for reinforced concrete slabs under punching loads. International Journal of Civil Engineering and Technology, 7 (3), 392-397.
15. Marzouk, H., & Hussein, A. (1991). Experimental investigation on the behavior of high-strength concrete slabs. ACI Structural Journal, 88(6), 701-713.
16. M. Said, A.A. Abd El-Azim, M.M. Ali, H. El-Ghazaly, I. Shaaban, Effect of elevated temperature on axially and eccentrically loaded columns containing Polyvinyl Alcohol (PVA) fibers, Eng. Struct. 204 (2020) 110065, https://doi.org/10.1016/j. engstruct.2019.110065.